TOWARDS CONTROLLABLE AND PHYSICAL INTERPRETABLE UNDERWATER SCENE SIMULATION

Kaixin Chen[1], Lin Zhang[1], Ying Shen[1], Yicong Zhou[2]*

[1]School of Software Engineering, Tongji University, Shanghai, China
[2]Department of Computer and Information Science, University of Macau, Macau, China

ABSTRACT

The realistic simulation of underwater scenes has important significance for many researches related to underwater vision, such as underwater image restoration, underwater moving object monitoring, etc. To date, however, the existing underwater scene simulation pipelines are either too complicated due to the continuous spectra and camera parameters involved, or difficult to control since the empirically controlled distance based fog effect is usually used by them. In this paper, we try to fill in this research gap by proposing an *U*nderwater *S*cene *Sim*ulation approach, namely USSim, which especially focuses on the influence of ocean water. In USSim, Jerlov water type and depth are regarded as main variables to control the simulation effects. In addition, the spectra of the incident light is decomposed into three primary components and their attenuations are modeled separately, and finally the simulated scene is generated via the hybrid underwater imaging model proposed by us. USSim greatly reduces the computational complexity and enables the fog effect to be controlled by variables with explicit physical meanings. The controllability, physical interpretability and simulation effects of our USSim under different conditions have been verified by extensive experiments. To make our results reproducible, the source code is made online available at https://cslinzhang.github.io/USSim/.

***Index Terms*—** Underwater Scene Simulation, Jerlov Water Types, Underwater Imaging Model

1. INTRODUCTION

Recent years have witnessed a growing interest in the exploration and researches on marine mineral resources [1] and biological populations [2] based on vision technologies. However, it is highly expensive and even impractical to get real underwater images in some cases. A feasible solution to conquer this problem is to use virtual simulation technologies to create realistic underwater scenes, which is also the focus of this paper.

From the theoretical perspective, the primary issue of simulating underwater images is how to model the imaging mechanism of the underwater object. The underwater optical imaging models related to the imaging mechanism can be roughly sorted into four categories [3], the point spread function model (PSFM) [4], the turbulence degradation model (TDM) [5], the Jaffe-McGlamery model (JMM) [6–8], and the foggy image degradation model (FIDM) [9, 10]. Among them, PSFM and TDM lack physical interpretability correlated with the optical properties of seawater, and thus is not suitable for the virtual simulation. JMM attempts to decompose the light received by the underwater camera. and is the most widely used underwater imaging model so far. However, because of different emphases in various usage scenarios [11–13], the formulas of JMM are not uniform when used. Therefore, it is necessary to simplify JMM when it is applied in underwater scene simulations. FIDM regards the underwater image as a linear superposition of the anhydrous scene and the water body. It is mainly used for dark channel prior based image dehazing. When FIDM works in an atmospheric environment, it can accurately estimate the optical distance from the camera to the object, but when applied to an underwater environment, it cannot accomplish this task well [14–16].

From the application aspect, the existing underwater scene simulation methods are mostly based on the FIDM and use distance fog effect in game engines [17, 18]. For example, in [17], Liarokapis *et al.* specify the fog effect's color and density empirically and calculate the loss and intensity of extra illumination by linear interpolation. Thompson *et al.* [18] directly extract the color of the fog effect from the reference photos. Although these application oriented methods are able to simulate underwater scenes, they share some common shortcomings, such as low controllability and lack of physical interpretability.

To solve the aforementioned problems in the application-oriented method, in this article, we propose a hybrid underwater imaging model and build a **U**nderwater **S**cene **Sim**ulation pipeline in Unity based on this model, named **USSim**. Our contribution can be summarized as follows:

1. A simulation-specific underwater optical imaging model is proposed to build the distance fog in the game engines rather than setting the distance fog empirically like other works, which ensures our simulation methods with strong physical interpretability.
2. We propose the simulation pipeline USSim, which to our knowledge, is the first underwater environment simulation pipeline in the game engines that applies the classification criteria of the Jerlov water types. As a result, our USSim can simulate underwater scenes independently without reference images.
3. We also propose a strategy to calculate the color of underwater ambient light. By decomposing the incident light into three primary rays using color matching function, we avoid the calculation of the entire continuous spectrum and thus reduce the computational complexity.

2. METHODOLOGY

In this section, the hybrid underwater imaging model which is the basis of USSim will be given first in Sec. 2.1. Then, in Sec. 2.2 the workflow of USSim will be presented briefly. Finally, in Sec. 2.3 we will introduce the details of method designed to calculate the color of underwater ambient light.

*Corresponding author: cslinzhang@tongji.edu.cn.

2.1. A Hybrid Underwater Imaging Model

The proposed hybrid underwater imaging model in this article is based on JMM [6–8] and FIDM [9, 10]. So, in this subsection, we first briefly introduce JMM and FIDM, and subsequently present our model.

Jaffe-Mcglamory Model. JMM divides the light received by the underwater camera in the line of sight E_T into three components: 1) the light directly reflected from the captured scene E_d, 2) the light that reaches the camera after being scattered by small particles E_f, and 3) the light from the atmosphere and reflected by suspended particles E_b. The relationship among these components and E_T conforms to,

$$E_T = E_d + E_f + E_b. \tag{1}$$

As when the objects are relatively close to the camera, E_f has less influence on underwater imaging than E_d and E_b, so like other studies [19], we ignore E_f and only consider the rest.

When the camera and the object are in the same horizontal plane, the received radiance of light E_T can be obtained by,

$$E_T = E(d, \lambda)e^{-\beta(\lambda)z} + B^{\infty}(\lambda)(1 - e^{-\beta(\lambda)z}), \tag{2}$$

where $E(d, \lambda)e^{-\beta(\lambda)z}$ represents the direct transmission light E_d using the Beer-Lambert law [20] and $B^{\infty}(\lambda)(1 - e^{-\beta(\lambda)z})$ denotes the backward scattering light E_b [21]; $d,\ \beta(\lambda),\ \lambda$, and z denote the depth, the attenuation coefficient, the wavelength of the light, and the distance of the optical path, respectively.

Foggy image degradation model. FIDM [9,10] is composed of two parts, the attenuation component and the ambient light component. It can be expressed as,

$$I(\mathbf{x}) = J(\mathbf{x}) \cdot t(\mathbf{x}) + A \cdot (1 - t(\mathbf{x})), \tag{3}$$

where $\mathbf{x}$ means the coordinate of a pixel in the image, A is a constant value of the ambient light from horizon sky, and $I(\cdot),\ J(\cdot)$, and $t(\cdot)$ return the foggy image, the fog-free image, and the transmittance, respectively.

Although according to [9], $t(\mathbf{x})$ is generally taken as $e^{-\beta z(\mathbf{x})}$ in the atmosphere, in different usage scenarios such as dark channel prior dehazing, $t(\mathbf{x})$ can also be calculated with other forms [14].

A hybrid underwater imaging model. From Eq. 2 and Eq. 3, we can have some useful findings that when combining the physical meaning of JMM with the form of FIDM and making $t = e^{-\beta(\lambda)z}$, we are able to construct a hybrid underwater imaging model which is formed as,

$$I(\lambda) = J(\lambda) \cdot e^{-\beta(\lambda)z} + A(\lambda) \cdot (1 - e^{-\beta(\lambda)z}), \tag{4}$$

where $I(\lambda)$ is the observed radiance representing the simulated underwater scene, $J(\lambda)$ is the anhydrous scene radiance, $A(\lambda)$ is the radiance of ambient light from backward scattering, $\beta(\lambda),\ \lambda$ and z are the same as defined in Eq. 2.

However, Eq. 4 is not suitable when simulating underwater scenes by distance fog in the game engines, since calculations can only be performed in the sRGB color space instead of the entire spectra. When we use Eq. 4 to simulate underwater scenes in RGB channels separately, if $\beta(\lambda)$ and $J(\lambda)$ are small, the simulation scenes will be reddish, which is unreasonable. Therefore, in practical applications, we simplify the Eq. 4 to the form as,

$$I(\mathbf{x}) = J(\mathbf{x}) \cdot e^{-\beta z(\mathbf{x})} + A \cdot (1 - e^{-\beta z(\mathbf{x})}), \tag{5}$$

where $I(\mathbf{x})$ is the RGB color at a certain coordinate in the imaging plane of the simulated underwater scene, $J(\mathbf{x})$ is the RGB color of the same coordinate in the anhydrous scene, A is the color of the ambient light, and β is a constant value of the attenuation coefficient. The methods of obtaining these variables will be introduced in the following content.

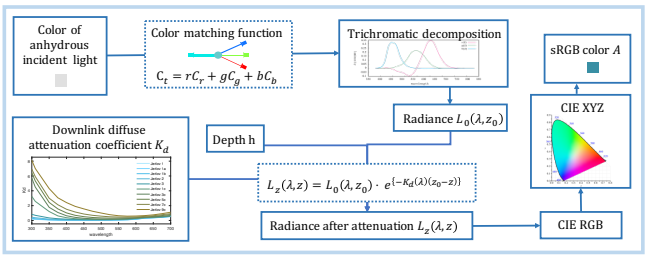

Fig. 1. The calculation of the underwater ambient light's color A involves three steps, color decomposition, attenuation calculation, and color space transformation. First, the color of anhydrous incident light is decomposed into the luminances of red, green, and blue. Second, these luminances are converted into radiances to perform the attenuation calculation. Lastly, the radiances are converted back to luminances to get coordinates in CIE RGB which are further transformed to sRGB to obtain A.

2.2. The Underwater Scene Simulation Workflow

Our USSim consists of three stages: anhydrous scene construction, ambient light's color calculation, and distance fog generation.

In the anhydrous scene construction stage, we build an anhydrous scene in the game engine and select an observation camera. Once the scene and the camera are determined, we can easily obtain the color of the anhydrous scene $J(\mathbf{x})$ and the distance from the target to the camera $z(\mathbf{x})$ at any pixel $\mathbf{x}$ in the imaging plane. In the ambient light's color calculation stage, we use the water type, the water depth, and the color of the incident light above the water surface as variables to calculate the color of the ambient light A, and use it as the color of the distance fog.

In the final stage of distance fog generation, we refer to Eq. 5, use $e^{-\beta z(\mathbf{x})}$ to present the density of the fog effect, and add it to the anhydrous scene to generate the underwater scene. To integrate the different degrees of attenuation of the three wavelengths of RGB by water, we use the following equation to calculate β as,

$$\beta = \frac{R}{R+G+B}\beta_R + \frac{G}{R+G+B}\beta_G + \frac{B}{R+G+B}\beta_B, \tag{6}$$

where (R, G, B) are the components of the ambient light's color A in the RGB channels, and $\beta_R,\ \beta_G$, and β_B are the attenuation coefficients in the case of the wavelengths of red, green, and blue light, which can be obtained from [22].

2.3. Derivation of the Underwater Ambient Light

From Sec. 2.2, A is the only undetermined variable in Eq. 5. To this end, we design a pipeline as shown in Fig. 1 to determine A. The three parts of the pipeline, the decomposition of light, the calculation of attenuation, and the conversion of the color space, will be introduced in this part.

2.3.1. Color Decomposition and Attenuation Calculation

Different wavelengths of light are attenuated differently, but simulating the attenuation of the entire continuous spectra is too com-

Table 1. Comparison of the controllable physical quantities.

	λ	z	d	E / L	K_d	β
Ours (USSim)	✓	✓	✓	✓	✓	✓
Liarokapis *et al.* [17]	✓	✗	✓	✗	✓	✗
Thompson *et al.* [18]	✗	✓	✗	✗	✗	✗

plicated and the data acquisition requirements are too high, so we consider disassembling the sunlight from a discrete perspective.

According to the color matching function [23], light of any color can be matched by the three primary colors, and the ratio of the three primary colors can be expressed as tristimulus values, which are the required luminosities of the three primary colors to achieve a color match. So we use the color matching function to convert the D65 standard daylight simulation as the incident light into tristimulus values $(Il_R,\ Il_G,\ Il_B)$ representing luminosities.

However, the luminosity is only a subjective concept, to get an absolute luminance, we must un-scale the values using a set of relative luminances via,

$$\begin{cases} r = Il_R \cdot Rl_r \\ g = Il_G \cdot Rl_g \\ b = Il_B \cdot Rl_b \end{cases}, \tag{7}$$

where $r,\ g$ and b are the luminances, $Rl_r\ =\ 1,\ Rl_g\ =\ 4.5907$ and $Rl_b\ =\ 0.0601$ mean the relative luminances.

The above-mentioned luminances are the intensity of light per unit area of their source. Since luminance is independent of energy, it cannot be directly used to calculate attenuation. So we need to convert $(r,\ g,\ b)$ to radiances $(L_r,\ L_g\ , L_b)$, which represent the radiant energy emitted per unit time in a specified direction by a unit area of an emitting surface, with a simple linear relationship [24]. Then, according to the definition of downward diffusion attenuation coefficient, the attenuation can be calculated via,

$$\begin{cases} L_{zr} = L_r \cdot e^{-K_{dr}d} \\ L_{zg} = L_g \cdot e^{-K_{dg}d} \\ L_{zb} = L_b \cdot e^{-K_{db}d} \end{cases}, \tag{8}$$

where d is the same as defined in Eq. 2; $K_{dr},\ K_{dg}$ and K_{db} are the coefficients of downward diffusion attenuation in the case of the wavelengths of red, green, and blue light. Furthermore, we convert $(L_{zr},\ L_{zg},\ L_{zb})$ back to luminances $(r_z,\ g_z,\ b_z)$ with a simple linear relationship [24].

As a result, by adopting the pipeline above, we can obtain the attenuation of the red, green, and blue components of the discrete sunlight, and get their luminances $(r_z,\ g_z,\ b_z)$ after the attenuation.

2.3.2. Color Space Transformation

To obtain a specific color A, we still need to transform the luminances of red, green, and blue in the color space CIE RGB to the color space sRGB.

The color space with RGB tristimulus values as coordinates is called CIE RGB. Because there are negative numbers in the color matching function [23], to facilitate the calculation, CIE proposed a three-dimensional conversion matrix M to adjust all the tristimulus values to positive numbers and thus construct CIE XYZ with all coordinates in the range [0,1].

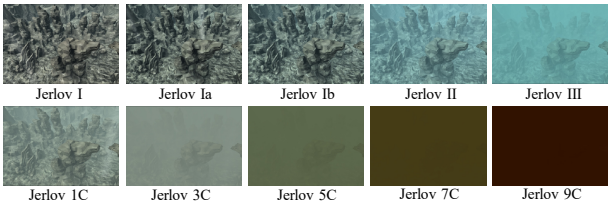

(a)

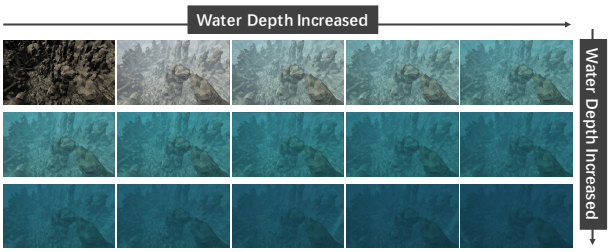

(b)

Fig. 2. (a) The simulation results of different Jerlov water types under the same water depth (3m). (b) The simulation outputs of the Jerlov II water with the depth from 0 to 14m. The depth gradually increases from left to right and from top to bottom.

So we use the conversion matrix M to convert our $(r_z,\ g_z,\ b_z)$ from Eq. 8 to the coordinate in CIE XYZ via,

$$[X\ Y\ Z]^T = M[r_z\ g_z\ b_z]^T. \tag{9}$$

As CIE XYZ is independent of the camera equipment, it needs to be further converted to sRGB for rendering. To fulfill this goal, we need to transform CIE XYZ to sRGB in two steps [25]. First, the unprocessed sRGB coordinates can be obtained by multiplying the CIE XYZ coordinates via,

$$[r_{raw}\ g_{raw}\ b_{raw}]^T = N[X\ Y\ Z]^T, \tag{10}$$

where $[r_{raw}, g_{raw}, b_{raw}]^T$ is the unprocessed coordinate of a point in sRGB and N is another conversion matrix. Second, the sRGB coordinates are obtained by a piecewise function,

$$A_c = \begin{cases} 12.92 c_{raw} & c_{raw} \le 0.0031308 \\ 1.055 c_{raw}^{\frac{1}{2.4}} - 0.055 & c_{raw} > 0.0031308 \end{cases}, \tag{11}$$

where c_{raw} is $r_{raw},\ g_{raw}$ or b_{raw}, A_c is $A_r,\ A_g$, or A_b and $A_c \in [0, 1]$, and $(A_r,\ A_g,\ A_b)$ are the values of RGB channels of A.

Using the above-presented pipeline, the color of underwater ambient light A can be determined according to the water types, the water depth, and the incident light. Consequently, Eq. 5 can be used to simulate the underwater color.

3. EXPERIMENTS AND DISCUSSIONS

In this section, we will evaluate the performance of our proposed USSim from both qualitative and quantitative experiments.

3.1. Qualitative Experiments

We performed our qualitative experiments from two aspects: controllability and simulation outputs.

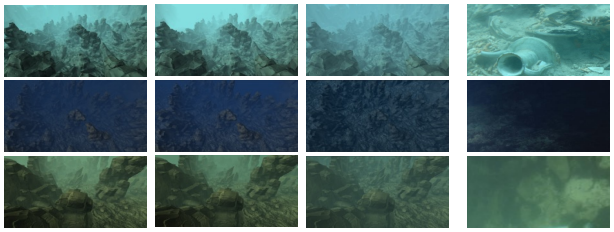

Fig. 3. Comparison of the underwater scene simulations. The images presented in (a)∼(c) are the simulation results of Liarokapis *et al.*'s [17], Thompson *et al.*'s [18] and our approaches, respectively. (d) Actual underwater images under similar conditions.

Table 2. Comparison of the average of image AuthESI values under oceanic and coastal conditions.

	oceanic AuthESI	coastal AuthESI
Real images	3.253	2.075
Ours (USSim)	**3.597**	**2.171**
Liarokapis *et al.* [17]	4.068	3.978
Thompson *et al.* [18]	4.532	5.350

Analysis on controllability. To evaluate the controllability and the ability of physical interpretation of the proposed USSim, according to [22] and [26], some commonly used physical quantities related to underwater imaging are analysed in this subsection. Among them, d, β, λ and z are the same as defined in Eq. 2, K_d is the same as defined in Eq. 8, and E (L) means the irradiance (radiance), which represents the energy of the light. Two representative underwater simulation piplines, Liarokapis *et al.*'s [17] and Thompson *et al.*'s [18], widely used in game engines, are compared with our method in terms of the above-mentioned physical quantities. The variable usage of each scheme is listed in Table 1.

As shown, our USSim involves more physical quantities. Among the three approaches in Table 1, both [17] and [18] use the distance based fog effect to simulate the underwater environment, but many of the quantities related to the fog effect is set empirically. Thus, their simulations lack diversity. Instead, our simulation outputs can be customized by changing the water type to adjust K_d and β, modulating d to control the attenuation, and regulating z to affect the fog effect's intensity, which makes our USSim more theoretical and practical, and also guarantees the controllability.

Simulation performance on underwater scene. Assuming that the incident light is D65 which is one of the standard daylight simulations, our underwater scene simulation results are illustrated in Fig. 2. Moreover, USSim was compared with two competitors [17, 18], with some simulation results and the samples listed in Fig. 3. All simulation results are generated in Unity 2020.3.18f1c1 LTS.

In Fig. 2 (a), we show the simulation results of different Jerlov water types. Jerlov categorized the ocean water into five oceanic types (I, IA, IB, II, and III) and five coastal types (1C, 3C, 5C, 7C, and 9C) in [27]. And in Fig. 2 (a), from left to right, the whole set of pictures of Fig. 2 (a) is the oceanic and the coastal water in the same sequences. As the water become more and more turbid, the simulated scene gradually changed from blue to yellow-green, and even to reddish brown. Fig. 2 (b) demonstrates some examples of the simulation outputs of the Jerlov II water type with depths ranging from 0 to 14m. As shown, with the water depth increasing, the brightness of the color changes greatly, and the hue changes slightly.

In addition, the simulation results of the methods in [17] and [18] as well as USSim under several underwater conditions are illustrated in Fig. 3, where each row of the images represents the simulation scenes and the sample photos under similar conditions. Since the source codes of [17] and [18] were unavailable, we reproduced these two methods according to their corresponding papers. Besides, we set the colors of their fog effects directly from the sample photos, and ignored some simulation skills such as the caustics, god rays, etc., which had little to do with the underwater imaging models. As shown in Fig. 3, it can be found that our USSim results appear smoother and more natural.

3.2. Quantitative Experiments

The real underwater environment is affected by many factors and has various characteristics in different regions, so there is still no perfect standard to quantify the quality of the simulations results. But considering that the distance fog is commonly used in game engines to simulate underwater scenes, we adopted the synthetic fog/hazy image realism evaluator (AuthESI for short) proposed in [28] to objectively evaluate the authenticity of the synthetic underwater images. A smaller AuthESI value indicates a more natural simulated image.

With the above knowledge, we designed a quantitative experiment. We divided underwater scenes into two types: oceanic environment and coastal environment. For each environment, we used our USSim to simulate 40 underwater images. The same operation was also applied to Liarokapis *et al.*'s method [17] and Thompson *et al.*'s method [18]. So there were 240 images in total. In addition, we collected 40 real underwater images for each environment as control groups. Then we calculated the images' AuthESI values and got the averages of the 8 groups. The results are summarized in Table 2, from which it can be seen that our USSim can generate better simulation results in both oceanic and coastal environment.

4. CONCLUSION

In this article, to simulate the underwater scene, we take the water type and the water depth as the main variables, decompose the spectra of the incident light and design a pipeline to determine the underwater ambient light, and propose a hybrid underwater imaging model to fulfill this goal. Meanwhile, extensive experiments verify the controllability of the proposed method. In addition, some underwater color simulation results and the quantitative comparison also demonstrate that our approach can perform well in underwater environment. In future research, we will devote our efforts to explore more factors that affect the color of underwater imaging.

5. ACKNOWLEDGMENT

This work was supported in part by the National Natural Science Foundation of China under Grants 61973235, 61936014, and 61972285, in part by the Natural Science Foundation of Shanghai under Grant 19ZR1461300, in part by the Shanghai Science and Technology Innovation Plan under Grant 20510760400, in part by the Dawn Program of Shanghai Municipal Education Commission under Grant 21SG23, in part by the Shanghai Municipal Science and Technology Major Project under Grant 2021SHZDZX0100, and in part by the Fundamental Research Funds for the Central Universities.

6. REFERENCES

[1] Norman Toro, Pedro Robles, and Ricardo I Jeldres, "Seabed mineral resources, an alternative for the future of renewable energy: A critical review," *Ore Geology Reviews*, vol. 126, pp. 103699, 2020.

[2] Huimin Lu, Tomoki Uemura, Dong Wang, Jihua Zhu, Zi Huang, and Hyoungseop Kim, "Deep-sea organisms tracking using dehazing and deep learning," *Mobile Networks and Applications*, vol. 25, no. 3, pp. 1008–1015, 2020.

[3] Miao Yang, Jintong Hu, Chongyi Li, Gustavo Rohde, Yixiang Du, and Ke Hu, "An in-depth survey of underwater image enhancement and restoration," *IEEE Access*, vol. 7, pp. 123638–123657, 2019.

[4] Weilin Hou, Deric J Gray, Alan D Weidemann, and Robert A Arnone, "Comparison and validation of point spread models for imaging in natural waters," *Optics Express*, vol. 16, no. 13, pp. 9958–9965, 2008.

[5] R.E. Hufnagel and N.R. Stanley, "Modulation transfer function associated with image transmission through turbulent media," *The Journal of the Optical Society of America*, vol. 54, no. 1, pp. 52–61, 1964.

[6] B.L. McGlamery, "Computer analysis and simulation of underwater camera system performance," *Scripps Institution of Oceanography Reference*, vol. 75, no. 2, 1975.

[7] B.L. McGlamery, "A computer model for underwater camera systems," in *Ocean Optics VI*, 1980.

[8] Jules S Jaffe, "Computer modeling and the design of optimal underwater imaging systems," *IEEE Journal of Oceanic Engineering*, vol. 15, no. 2, pp. 101–111, 1990.

[9] Earl J McCartney, *Optics of the Atmosphere: Scattering by Molecules and Particles*, John Wiley and Sons, Inc., New York, USA, 1976.

[10] Shree K Nayar and Srinivasa G Narasimhan, "Vision in bad weather," in *the Seventh IEEE International Conference on Computer Vision*, 1999.

[11] Emanuele Trucco and Adriana T Olmos-Antillon, "Self-tuning underwater image restoration," *IEEE Journal of Oceanic Engineering*, vol. 31, no. 2, pp. 511–519, 2006.

[12] John Y. Chiang and Ying-Ching Chen, "Underwater image enhancement by wavelength compensation and dehazing," *IEEE Transactions on Image Processing*, vol. 21, no. 4, pp. 1756–1769, 2012.

[13] Derya Akkaynak and Tali Treibitz, "A revised underwater image formation model," in *IEEE Conference on Computer Vision and Pattern Recognition*, 2018.

[14] Kaiming He, Jian Sun, and Xiaoou Tang, "Single image haze removal using dark channel prior," *IEEE Transactions on Pattern Analysis and Machine Intelligence*, vol. 33, no. 12, pp. 2341–2353, 2010.

[15] Adrian Galdran, David Pardo, Artzai Picón, and Aitor Alvarez-Gila, "Automatic red-channel underwater image restoration," *Journal of Visual Communication and Image Representation*, vol. 26, pp. 132–145, 2015.

[16] Paul Drews, Erickson Nascimento, Filipe Moraes, Silvia Botelho, and Mario Campos, "Transmission estimation in underwater single images," in *IEEE International Conference on Computer Vision Workshops*, 2013.

[17] Fotis Liarokapis, Pavel Kouřil, Panagiotis Agrafiotis, Stella Demesticha, Josef Chmelik, and Dimitrios Skarlatos, "3D modelling and mapping for virtual exploration of underwater archaeology assets," *The International Archives of the Photogrammetry, Remote Sensing and Spatial Information Sciences*, vol. XLII-2/W3, pp. 425–431, 2017.

[18] Stephen Thompson, Andrew Chalmers, and Taehyun Rhee, "Real-time mixed reality rendering for underwater 360 videos," in *IEEE International Symposium on Mixed and Augmented Reality*, 2019.

[19] Xinwei Zhao, Tao Jin, and Song Qu, "Deriving inherent optical properties from background color and underwater image enhancement," *Ocean Engineering*, vol. 94, pp. 163–172, 2015.

[20] Howard R Gordon, "Can the Lambert-Beer law be applied to the diffuse attenuation coefficient of ocean water?," *Limnology and Oceanography*, vol. 34, no. 8, pp. 1389–1409, 1989.

[21] Derya Akkaynak, Tali Treibitz, Tom Shlesinger, Yossi Loya, Raz Tamir, and David Iluz, "What is the space of attenuation coefficients in underwater computer vision?," in *IEEE Conference on Computer Vision and Pattern Recognition*, 2017.

[22] Michael G Solonenko and Curtis D Mobley, "Inherent optical properties of Jerlov water types," *Applied Optics*, vol. 54, no. 17, pp. 5392–5401, 2015.

[23] Hugh S Fairman, Michael H Brill, and Henry Hemmendinger, "How the CIE 1931 color-matching functions were derived from Wright-Guild data," *Color Research and Application*, vol. 22, no. 1, pp. 11–23, 1997.

[24] Alex Ryer, Ultraviolet Light, and Visible Light, "Light measurement handbook," Tech. Rep., International Light Inc., 1997.

[25] Matthew Anderson, Ricardo Motta, Srinivasan Chandrasekar, and Michael Stokes, "Proposal for a standard default color space for the internet-sRGB," in *Color and Imaging Conference*, 1996.

[26] Matthieu Boffety, Frédéric Galland, and Anne-Gaëlle Allais, "Color image simulation for underwater optics," *Applied Optics*, vol. 51, no. 23, pp. 5633–5642, 2012.

[27] Nils Gunnar Jerlov and Friedrich Franz Koczy, *Photographic Measurements of Daylight in Deep Water*, Elanders boktr., 1951.

[28] Ning Zhang, Lin Zhang, and Zaixi Cheng, "Towards simulating foggy and hazy images and evaluating their authenticity," in *International Conference on Neural Information Processing*, 2017.